Chinese Chemical Society | Xiamen University

Journal of Electrochemistry

Online First

6-14-2023

# Monodispersed Cu-TCPP/$Cu_2O$ hybrid microspheres: a superior cascade electrocatalyst towards $CO_2$ reduction to $C_2$ products

Zi-xuan Wan

Aidar Kuchkaev

Dmitry Yakhvarov

Xiong-wu Kang

COMMUNICATION

DOI: 10.13208/j.electrochem.2303271 Article ID: 1006-3471(2023)00-0000-00

Http://electrochem.xmu.edu.cn

# Monodispersed Cu-TCPP/$Cu_2O$ hybrid microspheres: a superior cascade electrocatalyst towards $CO_2$ reduction to $C_2$ products

Zi-xuan Wan [a], Aidar Kuchkaev [b], Dmitry Yakhvarov [b,c*], Xiong-wu Kang [a,*]

a New Energy Research Institute, School of Environment and Energy, South China University of Technology, Higher Education Mega Center, Guangzhou 510006, Guangdong, China

E-mail: Email: esxkang@scut.edu.cn; yakhvar@iopc.ru

b Arbuzov Institute of Organic and Physical Chemistry, FRC Kazan Scientific Center of RAS, Arbuzov Street 8, Kazan, 420088, Russian Federation

c Alexander Butlerov Institute of Chemistry, Kazan Federal University, Kremlyovskaya Street 18, Kazan, 420008, Russian Federation

**Abstract:** The electrochemical conversion of carbon dioxide into valuable chemicals is a feasible way to mitigate the negative impacts of overmuch carbon dioxide emissions. Porphyrin-based metal organic frameworks (MOFs) are expected to be used for selective and efficient electrochemical carbon dioxide reduction (ECR) with porous structure and ordered active sites. Herein, we report the synthesis of a monodispersed and spherical organic/inorganic hybrid Cu-TCPP@$Cu_2O$ electrocatalyst composed of Cu-TCPP (TCPP=tetrakis (4-carboxyphenyl) porphyrin) and $Cu_2O$, where TCPP play significant roles in regulating the morphology. In-situly formed Cu during ECR process in combination with Cu-TCPP (Cu-TCPP@Cu) can suppress hydrogen evolution, enrich CO intermediate and promote C-C coupling towards $C_2$ products. Cu-TCPP@Cu supported on porous carbon (PC) show ultrafine Cu nanoclusters on PC and displays high ECR activity and selectivity towards $C_2$ products, with a $C_2$ faradaic efficiency of 62.3% at –1.0 V versus the reversible hydrogen electrode (RHE) and a $C_2$ partial current density of 83.4 mA $cm^{-2}$, which is 7.6 times and 13.1 times that of pure $Cu_2O$ and TCPP. In this paper, the morphology and hybrid structure of the catalyst were studied to improve the selectivity of ECR to produce $C_2$ products, which provided a new idea for the design of high-performance ECR catalyst.

**Keywords:** organic/inorganic hybrid electrocatalysts; TCPP; cuprous oxide; cascade electrocatalysts

## 1. Introduction

Human activities lead to excessive emission of carbon dioxide ($CO_2$) into the atmosphere, resulting in serious environmental and climate problems, such as glacier melting and greenhouse effect[1-4]. Powerful methods of storing and converting $CO_2$ have been developed to reduce $CO_2$ levels in the atmosphere[5-8], among which, renewable energy driven electrocatalytic reduction of $CO_2$ (ECR) into valuable multi-carbon products is one of the promising and sustainable approaches[9-12]. However, catalysts limit the efficiency and selectivity of electrochemical $CO_2$ reduction[13-15]. Therefore, people have been committed to the development of a variety of efficient selective conversion of carbon dioxide electrocatalysts[16, 17], like metal oxides[18, 19], carbon-based materials[20] and metal organic frameworks (MOFs)[21, 22]. Despite the significant progress, it remains a huge challenge to direct the reaction path to the ideal product, which requires the development of better electrocatalysts with higher product selectivity and catalytic activity[23-25].

MOFs is regarded as an advantageous ECR electrocatalyst because of its porous crystalline structure and $CO_2$ affinities[26, 27]. Therefore, a large number of molecular catalysts combining transition metal elements (like Fe, Co, Ni, Mn and Cu) with macrocyclic ligands (such as polypyridine, porphyrins and phthalocyanine) have been examined for the electrochemical reduction of $CO_2$[28]. For instance, Chi and co-workers synthesized a kind of porous three-dimensional porphyrinic cobalt MOF with a CO faradaic efficiency of 92.4% at –0.6 V vs reversible hydrogen electrode (RHE)[29]. In addition, Kongpatpanich[30] prevented the aggregation of porphyrins by embedding functionalized cobalt-based and iron-based porphyrins into rigid frame structures and ensured the H bond interface was only close to the intermediate products of ECR at the same time, thus reducing the limit potential of ECR and improving the selectivity of ECR. Besides, Su's team synthesized a series of structurally stable metallic two-dimensional (2D) polyoxometale-metalloporphyrin organic frameworks (TM-PMOFs, TM = Fe, Co, Ni, Cu, Zn, Ru, Rh, Pd, Os, Ir, Pt). Their calculations showed that Lindqvist type clusters $[Mo_6]^{2e/2H}$ can act as a multi-electron regulator of the reduction reaction, reducing the drive potential of the reaction (0.08V)[31]. Unfortunately, considering the completion of the multi-electron transfer process required to obtain any reduced product in ECR, the poor conductivity and electron-donating capacity of MOF has always been a major limitation of MOF as an efficient electrocatalyst[32]. Therefore, it is imperative to design a novel catalyst with active components, electron-rich units and electron mobility.

At present, metals[33-35], metal sulfides [36] , organic groups [37] and metal oxides[38-40] have been combined with porphyrin

complexes to improve their activity and produce synergistic effects. Tetrakis (4-carboxyphenyl) porphyrin (TCPP) is a kind of electron donor which has been used to improve the ECR performances of MOFs[41]. Electron transfer could be facilitated by integrating electron-rich units into porphyrin-based MOFs, which could obtain excellent ECR activity. For example, Chang and colleagues reported a urea pendant modified molecular iron porphyrin catalyst with high CO faradic efficiency and the catalytic rate is 1500 times that of the unmodified parent iron porphyrin[42].

In addition, Zheng's group also developed a donor–acceptor modified Cu porphyrin (Cu-TAPP), which exhibits an excellent $CO_2$-to-$CH_4$ electroreduction performance, including a high $CH_4$ partial current density of 290.5 mA $cm^{-2}$ and a corresponding Faradaic efficiency of 54.8% at –1.63 V vs RHE in flow cells[43]. Liang's team[44] also synthesized nickel phthalocyanine (NiPc-MDE) with methoxy (-OMe) and cyanide (-CN). Compared with cyano-substituted NiPC-CN-MDE, the methoxy-substituted NiPC-OMe-MDE catalyst can stabilize *COOH intermediates and improve the selectivity of CO. NiPC-OMe-MDE catalyst can maintain 99.5% CO selectivity in the current density range of 10~300 mA $cm^{-2}$. Although these materials can effectively promote the catalysis of electrochemical reduction of $CO_2$, the ECR $C_2$ products are still very limited. Promoting the multi-electron transfer reactions with high selectivity of $C_2$ products remains a grand challenge for molecular-based electrocatalysts.

Herein, we report the deliberate synthesis of monodispersed and spherical organic/inorganic hybrid Cu-TCPP@$Cu_2O$, composed on 2-dimentional Cu-TCPP and $Cu_2O$, which is converted to Cu-TCPP@Cu during ECR process and displays a Faradic efficiency of 62.3 % at –1.0 V vs. RHE. Our study shows that the interaction between Cu-TCPP and $Cu_2O$ is the key factor contributing to its excellent ECR performance.

## 2. Experimental Section

### 2.1 Materials

Tetrakis (4-carboxyphenyl) porphyrin (TCPP, 97%), zinc nitrate hexahydrate ($Zn(NO_3)_2{\cdot}6H_2O$, 98%), Trifluoroacetic acid (99%) and copper nitrate trihydrate ($Cu(NO_3)_2{\cdot}3H_2O$, 99%) were purchased from Macklin. N, N-dimethylformamide (DMF, 99.9%), methanol, ethanol, 2-methylimidazole, potassium hydroxide (KOH, 95%) and polyvinylpyrrolidone (PVP, average mol wt 50,000) were purchased from Energy Chemical Co. Deionized water (DI, 18.2 MΩ·cm) was acquired from Milli-Q system. All agents were analytically pure and used without further purification.

### 2.2 Preparation of Cu-TCPP@$Cu_2O$ and contrastive samples

#### 2.2.1 Synthesis of Cu-TCPP@$Cu_2O$ nanoparticles

A solution of TCPP (20 mg, 0.025 mmol) and PVP (500 mg) in DMF (16 mL) was added to a solution of $Cu(NO_3)_2{\cdot}3H_2O$ (121.91 mg, 0.65 mmol) in DMF (10 mL). The solution was refluxed for 24 h at 120 ºC after stirring for 2 mins[45]. After cooling down to room temperature, the resulting red Cu-TCPP@$Cu_2O$ nanoparticles were washed four times with deionized water and collected by centrifuging at 8,500 rpm for 5 mins.

The synthesis process of pure $Cu_2O$ was the same as Cu-TCPP@$Cu_2O$ without TCPP.

The synthesis process of pure Cu-TCPP was the same as Cu-TCPP@$Cu_2O$ except for the addition of trifluoroacetic acid (20 μL, 1.0 M).

In addition, the catalysts after ECR corresponding to Cu-TCPP@$Cu_2O$, $Cu_2O$, Cu-TCPP and TCPP were named Cu-TCPP@Cu, OD-Cu, Cu-TCPP spent and TCPP spent, respectively. The samples mixed with porous carbon were named Cu-TCPP@$Cu_2O$/PC, $Cu_2O$/PC, Cu-TCPP/PC and TCPP/PC.

#### 2.2.2 Synthesis of porous carbon by carbonization of ZIF-8

The $Zn(NO_3)_2{\cdot}6H_2O$ (5.94 g, 0.02 mol) and 2-methylimidazole (6.56 g, 0.08 mol) was added into methanol (500 mL). After mixing with 12 h at room temperature, the formed ZIF-8 nanoparticles were washed for three times with methanol and collected by centrifuging at 8,500 rpm for 3 mins.

The ZIF-8 (500 mg) was put at a porcelain boat in a quartz tube furnace. Subsequently, the temperature of the tube furnace was elevated to 950 ºC with a heating rate of 5 ºC $min^{-1}$ under Ar atmosphere and held at this temperature for 3 h, the obtained porous carbon was named PC.

### 2.3 Morphological and structural characterization

Powder X-ray diffraction (Bruker D8 Advanced, German) was performed using a Cu Kα radiation source. X-ray photoelectron spectroscopy (XPS) were performed on a PHI X-tool X-ray photoelectron spectrometer using Al as the exciting source. Scanning electron microscopy (SEM) images and the element distribution of the catalyst were recorded using a Zeiss Supra 55. Transmission electron microscopy (TEM) image were performed in Talos F200x.

### 2.4 Electrochemical characterization

Electrochemical $CO_2$ reduction were performed on a CHI 660E electrochemical analyzer using a designed gas-tight flow cell. None of the electrochemical tests in this paper used IR compensation. The platinum foil counter electrode was purchased from Sigma Aldrich. The Hg/HgO reference electrode and carbon fiber paper was purchased from Gaoss Union. The conversion of the Hg/HgO electrode to the Reversible hydrogen electrode is performed using the following formula[46]:

$$E_{RHE} = E_{Hg/HgO} + 0.095\ V + 0.059\ \ pH$$

Firstly, a diluted Nafion solution was prepared by mixing 5 mL DI water, 5mL ethanol and 0.5 mL Nafion solution (5% w/w). Disperse 2.5 mg of Cu-TCPP@$Cu_2O$ catalyst and 2.5 mg PC into 5 mL of diluted Nafion solution, by sonication for 30 mins to obtain a catalyst ink. Drop-cast 1 mL the catalyst ink onto each carbon paper with gas diffusion layer (GDL) to obtain the catalyst-loaded gas diffusion electrode (GDE, 2 cm × 0.5 cm). The geometric area of each electrode is 1 $cm^2$ and the catalyst loading on each electrode was controlled to

be 1.0 mg $cm^{-2}$. The working electrodes for pristine $Cu_2O$/PC, Cu-TCPP/PC and TCPP/PC were prepared by following the same procedure as that of Cu-TCPP@$Cu_2O$/PC.

For all experiments, 1.0 M KOH (pH=14) solution was used as the electrolyte. The durability was evaluated by chronoamperometric profiles at a constant current density. The double-layer capacitance ($C_{dl}$) values and electrochemical surface area (ECSA) were determined by cyclic voltammetry (CV) curves at different scanning rates. Electrochemical impedance spectroscopy (EIS) measurements were obtained at frequencies ranging from 100 kHz to 0.01 Hz in a potentiostatic mode. Current densities were calculated based on the catalyst-covered geometric area of the working electrode. All potentials were referred to the reversible hydrogen electrode. The liquid product of ECR was quantified by $^1$H-NMR spectra recorded with an Agilent 400 MHz NMR instrument. The gas product generation of ECR was calculated by gas chromatography with an HuaAi GC-9560.

## 3. Results and Discussion

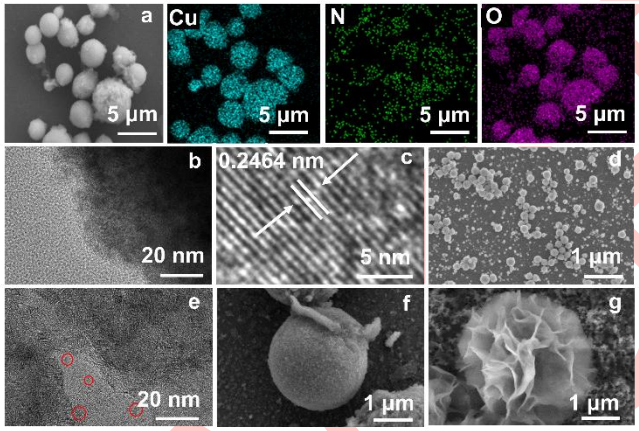


**Fig. 1.** The structural characterization: (a) SEM image of the Cu-TCPP@$Cu_2O$ and the corresponding EDX mapping of Cu, N, O, (b-c) TEM image of Cu-TCPP@$Cu_2O$ and (d) SEM image of $Cu_2O$, (e) TEM image of Cu-TCPP@Cu/PC, (f) SEM image of Cu-TCPP@Cu and (g) SEM image of Cu-TCPP.

The morphology of Cu-TCPP@$Cu_2O$ was examined by SEM and TEM. In Fig. 1a, Cu-TCPP@$Cu_2O$ exhibits a spherical shape and a bumpy surface, with a size of 2.78 ± 0.67 μm in diameter (Fig. S1a-b). It is highly possible that the bumpy surface of Cu-TCPP@$Cu_2O$ is assembled with ultra-thin nanosheet of Cu-TCPP[47]. The element mapping for Cu-TCPP@$Cu_2O$ demonstrates the uniform distribution of each element on the sample. The high-resolution TEM image of Cu-TCPP@$Cu_2O$ (Fig. 1b) further indicates the rough surface, composed of small nanoparticles at 3-5 nanometres. The lattice fringe at the heart of the sample were identified to be 0.2464 nm (Fig. 1c), which is in agreement with $Cu_2O$ (1 1 1) reflection[47]. Similarly, pristine $Cu_2O$ sample without TCPP functionalization equally shows spherical shape, and two size distributions in diameter, 96.56 and 264.74 nm respectively, which are much smaller than that of Cu-TCPP@Cu (Fig. 1d and Fig. S2a-c). This indicates that TCPP plays significant roles in regulating the morphology of $Cu_2O$.

After electrolysis at –1.0 V vs RHE for 30 mins, $Cu_2O$ were converted to metallic Cu, Cu nanoclusters with a diameter of about 3 nm on PC were observed for Cu-TCPP@Cu/PC sample (Fig. 1e). Fig. 1f indicate that Cu-TCPP@$Cu_2O$ retains its spherical structure even after electrolysis. In contrast, highly porous and aggregated Cu nanoparticles and nanowires at hundreds of nanometre scale were observed for pure $Cu_2O$ after electrolysis (OD-Cu, Fig S3a-3b). Apparently, Cu-TCPP can modulate not only the growth dynamics of $Cu_2O$, but also the recrystallization process of Cu during ECR process when $Cu_2O$ is converted to Cu. Due to the strong interaction of Cu-TCPP and Cu, the structure of Cu-TCPP@$Cu_2O$ was mainly maintained. SEM of Cu-TCPP fresh and Cu-TCPP spent (Fig. 1g and Fig. 3c-3d) also proves its structural stability. Cu-TCPP display a nanoflower-like structure. After electrolysis, the structure collapsed slightly but still maintained a flower-like structure in general. In Fig. S3e-3f, TCPP shows a severe aggregation both before and after electrolysis.

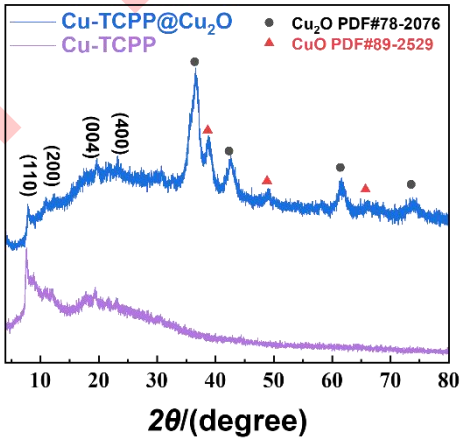


**Fig. 2.** XRD patterns of Cu-TCPP@Cu2O and Cu-TCPP.

As shown in Fig. 2 and Fig. S4, the peaks at 2θ values of 7.96, 11.03, 19.0 and 22.02° could be indexed to (110), (200), (004) and (400) reflection[47-50] of Cu-TCPP MOF in Cu-TCPP@$Cu_2O$ and Cu-TCPP both before and after electrolysis. The peaks at 36.52, 42.32, 61.43 and 73.34° correspond to the crystal planes of (111), (200), (220) and (311) of crystalline $Cu_2O$, respectively[51], which are observed for both Cu-TCPP@$Cu_2O$ and $Cu_2O$. In addition, the small peaks at 38.77, 48.84 and 65.73° might be indexed to CuO (PDF#89-2529).

$Cu^{2+}$ is possibly not completely converted into $Cu^+$ during the preparation of catalyst, thus a small amount of CuO remains in the catalyst. However, $Cu_2O$ is still dominant in the Cu-TCPP@$Cu_2O$. XRD results indicate that Cu-

TCPP@$Cu_2O$ represents Cu-TCPP functionalized $Cu_2O$, while only pure phase of $Cu_2O$ was obtained without using TCPP in the synthetic procedure. After electrolysis at –1.0 V vs RHE, the characteristic peak of $Cu_2O$ vanished in both Cu-TCPP@$Cu_2O$ and $Cu_2O$ and only diffraction peaks Cu was observed, signifying the complete conversion of $Cu_2O$ to Cu at the ECR process. However, the diffraction peaks of Cu-TCPP were well maintained during electrolysis, indicating its high stability against ECR process.

Fig. 3a shows the Cu 2*p* spectrum for as-prepared Cu-TCPP@$Cu_2O$. The binding energy at 932.5, 934.7 and 943.9 eV were assigned to $Cu^{1+}$ in $Cu_2O$, $Cu^{2+}$ in CuO and Cu-TCPP and the satellite of a Cu $2p_{3/2}$ peak, respectively[52, 53]. Three peaks appeared at 952.4, 954.6, and 963.4 eV were attributed to $Cu^{1+}$ in $Cu_2O$, $Cu^{2+}$ in CuO and Cu-TCPP and the satellite of a Cu $2p_{1/2}$ peak, respectively[45, 52, 53]. In Fig. 3b, the N 1*s* spectra of Cu-TCPP@$Cu_2O$/PC exhibit a peak at 400.3 eV and 398.8 eV, that could be accounted for pyridinic–N and Cu–N bond, respectively[50]. This further indicates the presence of Cu-TCPP in Cu-TCPP@$Cu_2O$ composite.As shown in Fig. 3c, after electrolysis, the satellite peak of Cu remains, which may come from $Cu^{2+}$ species in Cu-TCPP[50]. This further confirm the integrity of Cu-TCPP against ECR electrolysis.

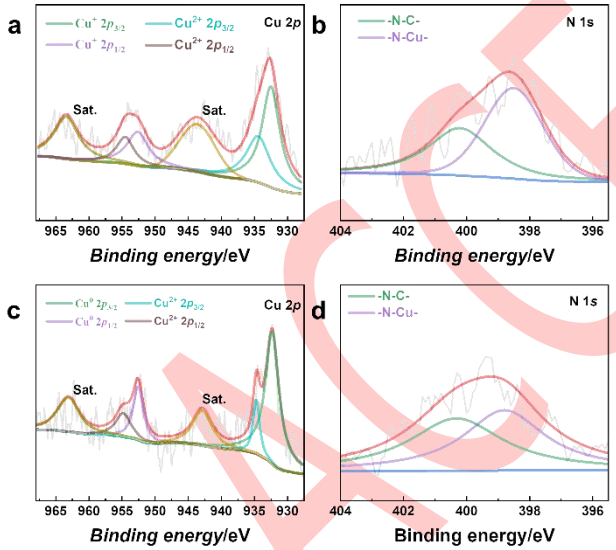


**Fig. 3.** XPS spectra of (a) Cu 2*p*, (b) N 1*s* for Cu-TCPP@$Cu_2O$/PC and (c) Cu 2*p*, (d) N 1*s* for Cu-TCPP@Cu/PC.

It should be also be noted that the intensity of the Cu oxide satellite peak becomes much weaker than that of the fresh sample due to conversion of $Cu_2O$ to Cu. The binding energy at 932.5 and 934.7 eV were assigned to $Cu^0$ and a few $Cu^{2+}$ in Cu-TCPP a Cu $2p_{3/2}$ peak[52-54]. Two peaks appeared at 952.4 and 954.6 eV were attributed to $Cu^0$ and a few $Cu^{2+}$ in Cu-TCPP a Cu $2p_{1/2}$ peak[43]. In Fig. 3d, the N 1*s* spectra of Cu-TCPP@Cu exhibit a higher peak intensity of pyridinic–N and lower peak intensity of Cu–N bond than Cu-TCPP@$Cu_2O$, possibly due to the partial breakage of Cu-N bond in Cu-TCPP and conversion to metallic Cu and TCPP[55-57]. However, according to XRD and SEM results, the Cu-TCPP structure in Cu-TCPP@$Cu_2O$ can generally remain stable after electrolysis.

The LSV (Fig. 4a) curves were recorded in $N_2$ and $CO_2$ atmosphere in 1.0 M KOH from 0 to –1.6 V vs. RHE. The current density of Cu-TCPP@$Cu_2O$/PC in $CO_2$ is higher than that in $N_2$, which indicates that catalyst does have ECR activity. It was found that the products distribution of ECR over TCPP@$Cu_2O$/PC depends on the electrode potential (Fig. 4b). At −0.8 V and −0.9 V vs RHE, $C_1$ product and $H_2$ dominate in ECR. As the catalyst electrode was further negatively polarized to −1.0 V, the yields of ethanol and ethylene dramatically increased, with ethylene being the dominant ECR product (Figure 4b). $C_2$ product is the predominant ECR product for the Cu-TCPP@$Cu_2O$/PC catalyst at –1.0 V vs. RHE (Fig. 4b) and its FE is 62.3%. In contrast, ECR is dominated by HER and CO on $Cu_2O$/PC (Fig. 4c), Cu-TCPP/PC (Fig. S5a) and TCPP/PC (Fig. S5b and Fig. S5c). These results indicate that the combination of $Cu_2O$ and Cu-TCPP on PC is essential for efficient production of $C_2$ products in ECR.

In Fig. 4d, Cu-TCPP@$Cu_2O$/PC displays a supreme partial current density of $C_2$ products in the potential range of –0.8 V to –1.0 V vs. RHE, which is as high as 83.4 mA $cm^{-2}$ and more than 7.6 times that of the unmodified $Cu_2O$, Cu-TCPP and TCPP. As shown in Fig. S5d and Fig. S6, the partial current density of $C_1$ (which is mainly CO) on Cu-TCPP@$Cu_2O$/PC is comparable to that of $Cu_2O$/PC and Cu-TCPP/PC but higher than TCPP/PC. It is further proved that the higher selectivity of $C_2$ product on Cu-TCPP@$Cu_2O$/PC is obtained by C-C coupling of a large number of CO intermediates on $Cu_2O$/PC and Cu-TCPP/PC. Tafel slopes are calculated based on Tafel equation ($\eta$ = b log $j$ + a, where $\eta$ is the overpotential, $j$ is the current density and b is the Tafel slope)[32] to elucidate the dynamics activity of catalyst for ECR (Fig. 4e). The Tafel slope for $C_2$ product on Cu-TCPP@$Cu_2O$/PC is 415.4 mV $dec^{-1}$, which is much smaller than that of $Cu_2O$/PC (1221.5 mV $dec^{-1}$), Cu-TCPP/PC (860.6 mV $dec^{-1}$) and TCPP/PC (692.1 mV $dec^{-1}$). The result states the favorable kinetics of Cu-TCPP@$Cu_2O$/PC for the formation of $C_2$ products.

It is highly possible that functionalization of OD-Cu with Cu-TCPP may enhance the hydrophobic properties of the catalyst composite, thus, suppressing the HER process. Additionally, both OD-Cu and Cu-TCPP here are good ECR catalysts for CO production and the combination of Cu-TCPP and OD-Cu possibly enhances the local concentration of CO intermediates on OD-Cu surface, thus, promoting C-C coupling for $C_2$ production. According to earlier report[58, 59], CO on Cu (2+) in Cu-TCPP and Cu (0) is also favorable to C-C coupling. All the three factors concurrently promote $C_2$ product in ECR process on Cu-TCPP@$Cu_2O$/PC catalyst. To examine the intrinsic activity of the catalysts, the electrochemical active surface area (ECSA) was evaluated by electrochemical double-layer capacitance ($C_{dl}$). Fig. S7-8 and Table S1 show that Cu-TCPP@$Cu_2O$/PC indeed exhibits larger $C_{dl}$ value and ECSA than that of $Cu_2O$/PC,

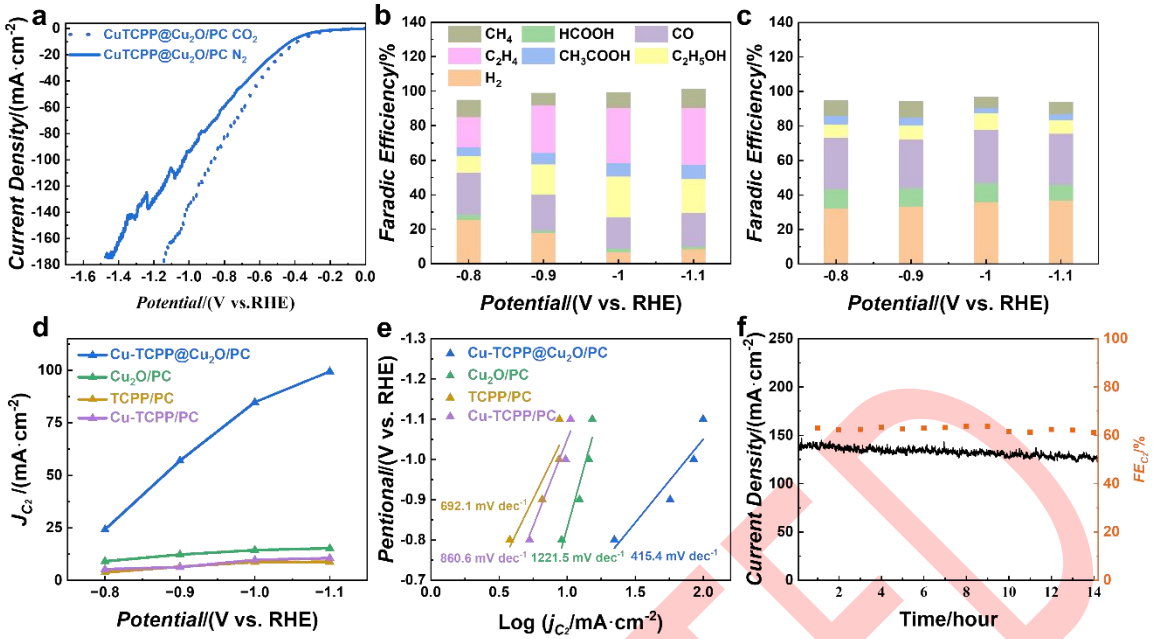


Cu-TCPP/PC and TCPP/PC, which provide more active sites in electrocatalyst to contact the electrolyte for ECR[29]. As shown in Fig. S9, the current density normalized to ECSA shows basically the same trend as in the geometric current density.

The Nyquist plots (Fig. S10) proves that Cu-TCPP @$Cu_2O$ /PC has much smaller charge transfer resistance $Cu_2O$/PC, Cu-TCPP/PC and TCPP/PC at the process of ECR, which indicates Cu-TCPP@$Cu_2O$/PC can provide faster electron transfer from the catalyst surface to the reactant in intermediate generation, eventually resulting in largely enhanced activity and selectivity[60, 61]. As shown in Fig.



**Fig. 4.** XPS spectra of (a) Cu 2*p*, (b) N 1*s* for Cu-TCPP@$Cu_2O$/PC and (c) Cu 2*p*, (d) N 1*s* for Cu-TCPP@Cu/PC.

4f, the faradaic efficiency of $C_2$ product is nearly 60% within 14 hours at a potential of –1.0V (vs. RHE), indicating an outstanding ECR stability.

## 4. Conclusion

In summary, we have successfully prepared uniformly distributed and spherical Cu-TCPP@$Cu_2O$ organic/inorganic hybrid catalysts, which is composed of 2-dimensional Cu-TCPP ultrathin nanosheet and $Cu_2O$. show excellent ECR performance towards production of $C_2$ products, with a faradic efficiency of 62.3% at a flow cell in 1.0 M KOH electrolyte. The Cu-TCPP@$Cu_2O$/PC catalyst has an inseparable interaction which can effectively adsorb the

intermediates as well as promoting the C-C coupling reaction and then improving the selectivity of $C_2$ products. This work highlights an effective strategy to design efficient Cu porphyrin-based MOF catalysts for electrochemical reduction of $CO_2$ into $C_2$ products.

.

## Acknowledgements

This work was supported by the National Natural Science Foundation of China (No. U2032151)

## Conflicts of interest

There are no conflicts to declare.

## References

[1] Wang W, Shang L, Chang G, Yan C, Shi R, Zhao Y, Waterhouse GIN, Yang D, Zhang T. Intrinsic Carbon-Defect-Driven Electrocatalytic Reduction of Carbon Dioxide[J]. Advanced Materials,2019, 31(19): 1808276.

[2] Luo T, Liu K, Fu J, Chen S, Li H, Pan H, Liu M. Electric Double Layer Structure in Electrocatalytic Carbon Dioxide Reduction[J]. Advanced Energy and Sustainability Research, 2022, 4(3): 2200148.

[3] Mu Z, Han N, Xu D, Tian B, Wang F, Wang Y, Sun Y, Liu C, Zhang P, Wu X, Li Y, Ding M. Critical Role of Hydrogen Sorption Kinetics in Electrocatalytic $CO_2$ Reduction Revealed by on-Chip in Situ Transport Investigations[J]. Nature Communications,2022, 13(1): 6911.

[4] Faunce TA, Lubitz W, Rutherford AW, MacFarlane D, Moore GF, Yang P, Nocera DG, Moore TA, Gregory DH, Fukuzumi S, Yoon KB, Armstrong FA, Wasielewski MR, Styring S. Energy and Environment Policy Case for a Global Project on Artificial Photosynthesis[J]. Energy & Environmental Science,2013, 6(3): 695-698.

[5] Masel RI, Liu Z, Yang H, Kaczur JJ, Carrillo D, Ren S, Salvatore D, Berlinguette CP. An Industrial Perspective on Catalysts for Low-Temperature $CO_2$ Electrolysis[J]. Nature Nanotechnology,2021, 16(2): 118-128.

[6] Zhou Y, Ni G, Wu K, Chen Q, Wang X, Zhu W, He Z, Li H, Fu J, Liu M. Porous Zn Conformal Coating on Dendritic-Like Ag with Enhanced Selectivity and Stability for $CO_2$ Electroreduction to CO[J]. Advanced Sustainable Systems,2023, 7(1): 2200374.

[7] De Luna P, Quintero-Bermudez R, Dinh C-T, Ross MB, Bushuyev OS, Todorović P, Regier T, Kelley SO, Yang P, Sargent EH. Catalyst Electro-Redeposition Controls Morphology and Oxidation State for Selective Carbon Dioxide Reduction[J]. Nature Catalysis,2018, 1(2): 103-110.

[8] Pan B, Fan J, Zhang J, Luo Y, Shen C, Wang C, Wang Y, Li Y. Close to 90% Single-Pass Conversion Efficiency for $CO_2$ Electroreduction in an Acid-Fed Membrane Electrode Assembly[J]. ACS Energy Letters,2022, 7(12): 4224-4231.

[9] Wu Y, Jiang Z, Lu X, Liang Y, Wang H. Domino Electroreduction of $CO_2$ to Methanol on a Molecular Catalyst[J]. Nature,2019, 575(7784): 639-642.

[10] Wang Q, Liu K, Hu K, Cai C, Li H, Li H, Herran M, Lu Y-R, Chan T-S, Ma C, Fu J, Zhang S, Liang Y, Cortés E, Liu M. Attenuating Metal-Substrate Conjugation in Atomically Dispersed Nickel Catalysts for Electroreduction of $CO_2$ to CO[J]. Nature Communications,2022, 13(1): 6082.

[11] Zhao S, Yang Y, Tang Z. Insight into Structural Evolution, Active Sites, and Stability of Heterogeneous Electrocatalysts[J]. Angewandte Chemie International Edition,2022, 61(11): e202110186.

[12] Pei-Xuan Liu, Lu-Wei Peng, Rui-Nan He, Lu-Lu Li, Jin-Li Qiao. A High-Performance Continuous-Flow MEA Reactor for Electroreduction $CO_2$ to Formate[J]. Journal of Electrochemistry, 2022, 28(1): 2104231.

[13] Wang Y-R, Yang R-X, Chen Y, Gao G-K, Wang Y-J, Li S-L, Lan Y-Q. Chloroplast-Like Porous Bismuth-Based Core–Shell Structure for High Energy Efficiency $CO_2$ Electroreduction[J]. Science Bulletin,2020, 65(19): 1635-1642.

[14] Tan D, Cui C, Shi J, Luo Z, Zhang B, Tan X, Han B, Zheng L, Zhang J, Zhang J. Nitrogen-Carbon Layer Coated Nickel Nanoparticles for Efficient Electrocatalytic Reduction of Carbon Dioxide[J]. Nano Research,2019, 12(5): 1167-1172.

[15] Hori Y, Wakebe H, Tsukamoto T, Koga O. Electrocatalytic Process of Co Selectivity in Electrochemical Reduction of $CO_2$ at Metal Electrodes in Aqueous Media[J]. Electrochimica Acta,1994, 39(11): 1833-1839.

[16] Deng P, Yang F, Wang Z, Chen S, Zhou Y, Zaman S, Xia BY. Metal–Organic Framework-Derived Carbon Nanorods Encapsulating Bismuth Oxides for Rapid and Selective $CO_2$ Electroreduction to Formate[J]. Angewandte Chemie International Edition,2020, 59(27): 10807-10813.

[17] Li Q, Fu J, Zhu W, Chen Z, Shen B, Wu L, Xi Z, Wang T, Lu G, Zhu J-j, Sun S. Tuning Sn-Catalysis for Electrochemical Reduction of $CO_2$ to CO Via the Core/Shell Cu/$SnO_2$ Structure[J]. Journal of the American Chemical Society,2017, 139(12): 4290-4293.

[18] Gao S, Lin Y, Jiao X, Sun Y, Luo Q, Zhang W, Li D, Yang J, Xie Y. Partially Oxidized Atomic Cobalt Layers for Carbon Dioxide Electroreduction to Liquid Fuel[J]. Nature,2016, 529(7584): 68-71.

[19] Zhang L, Zhao Z-J, Gong J. Nanostructured Materials for Heterogeneous Electrocatalytic $CO_2$ Reduction and Their Related Reaction Mechanisms[J]. Angewandte Chemie International Edition,2017, 56(38): 11326-11353.

[20] Han S-G, Ma D-D, Zhu Q-L. Atomically Structural Regulations of Carbon-Based Single-Atom Catalysts for Electrochemical $CO_2$ Reduction[J]. Small Methods,2021, 5(8): 2100102.

[21] Du D-Y, Qin J-S, Li S-L, Su Z-M, Lan Y-Q. Recent Advances in Porous Polyoxometalate-Based Metal–Organic Framework Materials[J]. Chemical Society Reviews,2014, 43(13): 4615-4632.

[22] Qin JS, Du DY, Guan W, Bo XJ, Li YF, Guo LP, Su ZM, Wang YY, Lan YQ, Zhou HC. Ultrastable Polymolybdate-Based Metal-Organic Frameworks as Highly Active Electrocatalysts for Hydrogen Generation from Water[J]. Journal of the American Chemical Society, 2015, 137(22): 7169–7177.

[23] Peng C, Zhu X, Xu Z, Yan S, Chang LY, Wang Z, Zhang J, Chen M, Sham T-K, Li Y, Zheng G. Lithium Vacancy-Tuned [$CuO_4$] Sites for Selective $CO_2$ Electroreduction to $C_{2+}$ Products[J]. Small,2022, 18(8): 2106433.

[24] Qian Guo, Jia-Long Fu, Cheng-Yan Zhang, Chao-Yue Cai, Cheng Wang, Li-Hua Zhou, Rui-Bo Xu, Ming-Yan Wang. Preparation of CoO/RGO@Ni Foam Electrode and Its Electrocatalytic Reduction of $CO_2$[J]. Journal of Electrochemistry, 2021, 27(4): 449-455.

[25] Zhu Chang, Chen Wei, Song Yan-fang, Dong Xiao, Li Gui-hua, Wei Wei, Sun Yu-han. Effect of Reaction Conditions on Cu - Catalyzed $CO_2$ Electroreduction[J]. Journal of Electrochemistry, 2020, 26(6): 797-807.

[26] Liang Z, Qu C, Guo W, Zou R, Xu Q. Pristine Metal–Organic Frameworks and Their Composites for Energy Storage and Conversion[J]. Advanced Materials,2018, 30(37): 1702891.

[27] Kornienko N, Zhao Y, Kley CS, Zhu C, Kim D, Lin S, Chang CJ, Yaghi OM, Yang P. Metal–Organic Frameworks for Electrocatalytic Reduction of Carbon Dioxide[J]. Journal of the American Chemical Society,2015, 137(44): 14129-14135.

[28] Savéant J-M. Molecular Catalysis of Electrochemical Reactions. Mechanistic Aspects[J]. Chemical Reviews,2008, 108(7): 2348-2378.

[29] Chi S-Y, Chen Q, Zhao S-S, Si D-H, Wu Q-J, Huang Y-B, Cao R. Three-Dimensional Porphyrinic Covalent Organic Frameworks for Highly Efficient Electroreduction of Carbon Dioxide[J]. Journal of Materials Chemistry A,2022, 10(9): 4653-4659.

[30] Wannakao SA-O, Jumpathong W, Kongpatpanich KA-O. Tailoring Metalloporphyrin Frameworks for an Efficient Carbon Dioxide Electroreduction: Selectively Stabilizing Key Intermediates with H-Bonding Pockets[J]. Inorganic Chemistry, 2017, 56(12): 7200-7209.

[31] Wang C, Zhu C-Y, Zhang M, Geng Y, Li Y-G, Su Z-M. An Intriguing Window Opened by a Metallic Two-Dimensional Lindqvist-Cobaltporphyrin Organic Framework as an Electrochemical Catalyst for the $CO_2$ Reduction Reaction[J]. Journal of Materials Chemistry A,2020, 8(29): 14807-14814.

[32] Wang Y-R, Huang Q, He C-T, Chen Y, Liu J, Shen F-C, Lan Y-Q. Oriented Electron Transmission in Polyoxometalate-Metalloporphyrin Organic Framework for Highly Selective Electroreduction of $CO_2$[J]. Nature Communications,2018, 9(1): 4466.

[33] Hod I, Sampson MD, Deria P, Kubiak CP, Farha OK, Hupp JT. Fe-Porphyrin-Based Metal–Organic Framework Films as High-Surface Concentration, Heterogeneous Catalysts for Electrochemical Reduction of $CO_2$[J]. ACS Catalysis,2015, 5(11): 6302-6309.

[34] Titi HM, Patra R, Goldberg I. Exploring Supramolecular Self-Assembly of Tetraarylporphyrins by Halogen Bonding: Crystal Engineering with Diversely Functionalized Six-Coordinate $Tin(L)_2$–Porphyrin Tectons[J]. Chemistry – A European Journal,2013, 19(44): 14941-14949.

[35] Li J, Zeng H, Dong X, Ding Y, Hu S, Zhang R, Dai Y, Cui P, Xiao Z, Zhao D, Zhou L, Zheng T, Xiao J, Zeng J, Xia C. Selective $CO_2$ Electrolysis to CO Using Isolated Antimony Alloyed Copper[J]. Nature Communications,2023, 14(1): 340.

[36] He T, Chen S, Ni B, Gong Y, Wu Z, Song L, Gu L, Hu W, Wang X. Zirconium–Porphyrin-Based Metal–Organic Framework Hollow Nanotubes for Immobilization of Noble-Metal Single Atoms[J]. Angewandte Chemie International Edition,2018, 57(13): 3493-3498.

[37] Jin S, Son H-J, Farha OK, Wiederrecht GP, Hupp JT. Energy Transfer from Quantum Dots to Metal–Organic Frameworks for Enhanced Light Harvesting[J]. Journal of the American Chemical Society,2013, 135(3): 955-958.

[38] Modak A, Nandi M, Mondal J, Bhaumik A. Porphyrin Based Porous Organic Polymers: Novel Synthetic Strategy and Exceptionally High $CO_2$ Adsorption Capacity[J]. Chemical Communications,2012, 48(2): 248-250.

[39] Liu C, Zhang M, Li J, Xue W, Zheng T, Xia C, Zeng J. Nanoconfinement Engineering over Hollow Multi-Shell Structured Copper Towards Efficient Electrocatalytical C−C Coupling[J]. Angewandte Chemie International Edition,2022, 61(3): e202113498.

[40] Xue Teng, Yanli Niu, Shuaiqi Gong, Xuan Liu, Zuofeng Chen. Selective $CO_2$ Reduction to Formate on Heterostructured $Sn/SnO_2$ Nanoparticles Promoted by Carbon Layer Networks[J]. Journal of Electrochemistry, 2022, 28(2): 2108441.

[41] Gong L, Gao Y, Wang Y, Chen B, Yu B, Liu W, Han B, Lin C, Bian Y, Qi D, Jiang J. Efficient Electrocatalytic Carbon Dioxide Reduction with Tetraphenylethylene- and Porphyrin-Based Covalent Organic Frameworks[J]. Catalysis Science & Technology,2022, 12(21): 6566-6571.

[42] Derrick JS, Loipersberger M, Nistanaki SK, Rothweiler AV, Head-Gordon M, Nichols EM, Chang CJ. Templating Bicarbonate in the Second Coordination Sphere Enhances Electrochemical $CO_2$ Reduction Catalyzed by Iron Porphyrins[J]. Journal of the American Chemical Society,2022, 144(26): 11656-11663.

[43] Yu P, Lv X, Wang Q, Huang H, Weng W, Peng C, Zhang L, Zheng G. Promoting Electrocatalytic $CO_2$ Reduction to $CH_4$ by Copper Porphyrin with Donor–Acceptor Structures[J]. Small,2022, 19(4): 2205730.

[44] Zhang X, Wang Y, Gu M, Wang M, Zhang Z, Pan W, Jiang Z, Zheng H, Lucero M, Wang H, Sterbinsky GE, Ma Q, Wang Y-G, Feng Z, Li J, Dai H, Liang Y. Molecular Engineering of Dispersed Nickel Phthalocyanines on Carbon Nanotubes for Selective $CO_2$ Reduction[J]. Nature Energy,2020, 5(9): 684-692.

[45] Li B, Wang X, Chen L, Zhou Y, Dang W, Chang J, Wu C. Ultrathin Cu-TCPP MOF Nanosheets: A New Theragnostic Nanoplatform with Magnetic Resonance/near-Infrared Thermal Imaging for Synergistic Phototherapy of Cancers[J]. Theranostics,2018, 8(15): 4086-4096.

[46] Feng L-L, Yu G, Wu Y, Li G-D, Li H, Sun Y, Asefa T, Chen W, Zou X. High-Index Faceted $Ni_3S_2$ Nanosheet Arrays as Highly Active and Ultrastable Electrocatalysts for Water Splitting[J]. Journal of the American Chemical Society,2015, 137(44): 14023-14026.

[47] Zhao M, Wang Y, Ma Q, Huang Y, Zhang X, Ping J, Zhang Z, Lu Q, Yu Y, Xu H, Zhao Y, Zhang H. Ultrathin 2D Metal–Organic Framework Nanosheets[J]. Advanced Materials,2015, 27(45): 7372-7378.

[48] Li J, Song S, Meng J, Tan L, Liu X, Zheng Y, Li Z, Yeung KWK, Cui Z, Liang Y, Zhu S, Zhang X, Wu S. 2D MOF Periodontitis Photodynamic Ion Therapy[J]. Journal of the American Chemical Society,2021, 143(37): 15427-15439.

[49] La DD, Thi HPN, Kim YS, Rananaware A, Bhosale SV. Facile Fabrication of Cu(II)-Porphyrin MOF Thin Films from Tetrakis(4-Carboxyphenyl)Porphyrin and $Cu(OH)_2$ Nanoneedle Array[J]. Applied Surface Science,2017, 424: 145-150.

[50] Zhao S, Li S, Zhao Z, Su Y, Long Y, Zheng Z, Cui D, Liu Y, Wang C, Zhang X, Zhang Z. Microwave-Assisted Hydrothermal Assembly of 2d Copper-Porphyrin Metal-Organic Frameworks for the Removal of Dyes and Antibiotics from Water[J]. Environmental Science and Pollution Research,2020, 27(31): 39186-39197.

[51] Kooti M. Fabrication of Nanosized Cuprous Oxide Using Fehling's Solution[J]. Transaction F: Nanotechnology,2010, 17: 73.

[52] Karapinar D, Zitolo A, Huan TN, Zanna S, Taverna D, Galvão Tizei LH, Giaume D, Marcus P, Mougel V, Fontecave M. Carbon-Nanotube-Supported Copper Polyphthalocyanine for Efficient and Selective Electrocatalytic $CO_2$ Reduction to CO[J]. ChemSusChem,2020, 13(1): 173-179.

[53] Xu T, Wei S, Zhang X, Zhang D, Xu Y, Cui X. Sulfur-Doped $Cu_3p$ | S Electrocatalyst for Hydrogen Evolution Reaction[J]. Materials Research Express,2019, 6(7): 075501.

[54] Zhang J, Mao X, Pan B, Xu J, Ding X, Han N, Wang L, Wang Y, Li Y. Surface Promotion of Copper Nanoparticles with Alumina Clusters Derived from Layered Double Hydroxide Accelerates $CO_2$ Reduction to Ethylene in Membrane Electrode Assemblies[J]. Nano Research,2022.

[55] Mette G, Sutter D, Gurdal Y, Schnidrig S, Probst B, Iannuzzi M, Hutter J, Alberto R, Osterwalder J. From Porphyrins to Pyrphyrins: Adsorption Study and Metalation of a Molecular Catalyst on Au(111)[J]. Nanoscale, 2016,8: 7958-7968.

[56] Mei B, Liu C, Li J, Gu S, Du X, Lu S, Song F, Xu W, Jiang Z. Operando Herfd-Xanes and Surface Sensitive Δμ Analyses Identify the Structural Evolution of Copper(II) Phthalocyanine for Electroreduction of $CO_2$[J]. Journal of Energy Chemistry,2022, 64: 1-7.

[57] Tang J-K, Zhu C-Y, Jiang T-W, Wei L, Wang H, Yu K, Yang C-L, Zhang Y-B, Chen C, Li Z-T, Zhang D-W, Zhang L-M. Anion Exchange-Induced Single-Molecule Dispersion of Cobalt Porphyrins in a Cationic Porous Organic Polymer for Enhanced Electrochemical $CO_2$ Reduction Via Secondary-Coordination Sphere Interactions[J]. Journal of Materials Chemistry A,2020, 8(36): 18677-18686.

[58] Wang W, Deng C, Xie S, Li Y, Zhang W, Sheng H, Chen C, Zhao J. Photocatalytic C–C Coupling from Carbon Dioxide Reduction on Copper Oxide with Mixed-Valence Copper(I)/Copper(II)[J]. Journal of the American Chemical Society,2021, 143(7): 2984-2993.

[59] Sang J, Wei P, Liu T, Lv H, Ni X, Gao D, Zhang J, Li H, Zang Y, Yang F, Liu Z, Wang G, Bao X. A Reconstructed $Cu_2P_2O_7$ Catalyst for Selective $CO_2$ Electroreduction to Multicarbon Products[J]. Angewandte Chemie International Edition,2022, 61(5): e202114238.

[60] Lin Z, Jiang Z, Yuan Y, Li H, Wang H, Tang Y, Liu C, Liang Y. Cobalt-$N_4$ Macrocyclic Complexes for Heterogeneous Electrocatalysis of the $CO_2$ Reduction Reaction[J]. Chinese Journal of Catalysis,2022, 43(1): 104-109.

[61] Dylan Siltamaki, Shuai Chen, Farnood Rahmati, Jacek Lipkowski, Ai-Cheng Chen. Synthesis and Electrochemical Study of CuAu Nanodendrites for $CO_2$ Reduction[J]. Journal of Electrochemistry, 2021, 27(3): 278-290.

**Entry for the Table of Contents**

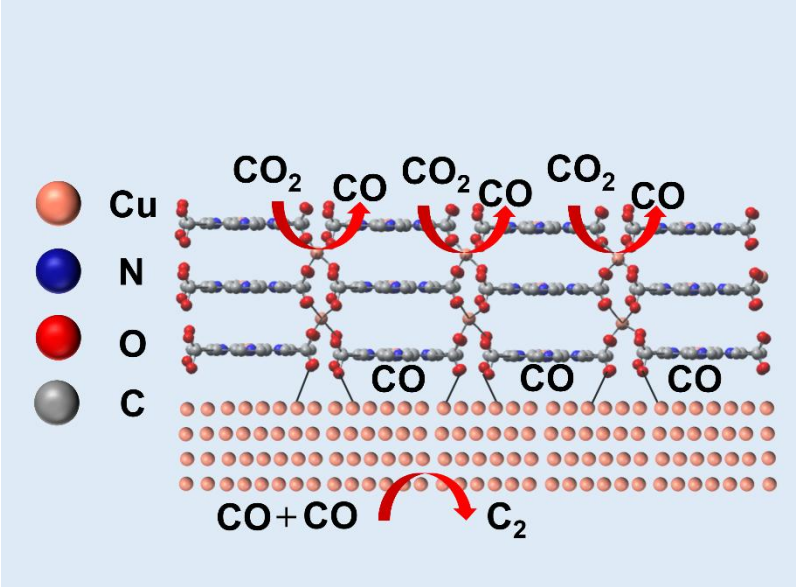

# 单分散 Cu-TCPP/$Cu_2O$ 杂化微球:一种具有优异电还原 $CO_2$ 产 $C_2$ 性能的级联电催化剂

万紫轩[a]，Aidar Kuchkaev[b]，Dmitry Yakhvarov[b,c*]，康雄武[a*]

（a. 华南理工大学环境与能源学院新能源研究所，广东，广州，510006；b. 阿尔布佐夫有机与物理化学研究所，俄罗斯联邦，俄罗斯联邦喀山市，喀山阿尔布佐夫街 8 号， 420088；c. 喀山联邦大学亚历山大·巴特列罗夫化学研究所，俄罗斯联邦， 喀山，克里姆廖夫斯卡亚街 18 号， 420008）

**摘要：**高效电还原 $CO_2$（ECR）为有价值的多碳产物是解决 $CO_2$ 排放问题的有效解决方案。基于卟啉的金属有机框架（MOFs）具有多孔结构和有序的活性位点，有望提高 ECR 生成多碳 产物的选择性。本文制备了由铜-四(4-羧基)卟啉（Cu-TCPP）和 $Cu_2O$ 组成的有机/无机杂化 Cu-TCPP@$Cu_2O$ 电催化剂，其中 TCPP 在调控形貌方面起着重要作用。ECR 过程中原位形成的 Cu 与 Cu-TCPP（Cu-TCPP@Cu）结合可以抑制析氢，富集 CO 中间体，促进 C-C 偶联生成 $C_2$ 产物。多孔碳（PC） 负载的 Cu-TCPP@Cu 在 PC 上被还原为 Cu 纳米簇，同时对 $C_2$ 产物具有较高的 ECR 活性和选择性。催化 剂在–1.0 V 时（相对于可逆氢电极），$C_2$ 产物法拉第效率为 62.3%，部分电流密度为 83.4 mA $cm^{-2}$，是纯 $Cu_2O$ 和 TCPP 的 7.6 倍和 13.1 倍。本论文研究了催化剂形貌和杂化结构如何提高 ECR 生成 $C_2$ 产物的选择性，为高性能 ECR 催化剂的设计提供了新思路。

**关键词：**有机/无机杂化电催化剂；四(4-羧基)卟啉；氧化亚铜；级联电催化剂